HHS Public Access

Author manuscript

Nat Med. Author manuscript; available in PMC 2020 February 01.

Published in final edited form as:

Nat Med. 2019 February ; 25(2): 277–283. doi:10.1038/s41591-018-0304-3.

Serum neurofilament dynamics predicts neurodegeneration and clinical progression in presymptomatic Alzheimer's disease

A full list of authors and affiliations appears at the end of the article.

Abstract

Neurofilament light chain (NfL) is a promising fluid biomarker of disease progression for various cerebral proteopathies. Here we leverage the unique characteristics of the Dominantly Inherited Alzheimer Network and ultrasensitive immunoas-say technology to demonstrate that NfL levels in the cerebrospinal fluid (n = 187) and serum (n = 405) are correlated with one another and are elevated at the presymptomatic stages of familial Alzheimer's disease. Longitudinal, within-person analysis of serum NfL dynamics (n = 196) confirmed this elevation and further revealed that the rate of change of serum NfL could discriminate mutation carriers from non-mutation carriers almost a decade earlier than cross-sectional absolute NfL levels (that is, 16.2 versus 6.8 years before the estimated symptom onset). Serum NfL rate of change peaked in participants converting from the presymptomatic to the symptomatic stage and was associated with cortical thinning assessed by magnetic resonance imaging, but less so with amyloid-β deposition or glucose metabolism (assessed by positron emission tomography). Serum NfL was predictive for both the rate of cortical thinning and cognitive changes assessed by the Mini–Mental State Examination and Logical Memory test. Thus, NfL dynamics in serum predict disease progression and brain neurodegeneration at the early presymptomatic stages of familial Alzheimer's disease, which supports its potential utility as a clinically useful biomarker.

*Correspondence and requests for materials should be addressed to M.J. mathias.jucker@uni-tuebingen.de.

Author contributions

All authors were involved in sample and data collection. J.K., O.P., A.A., S.A.K., and C.B. performed the immunoassay work. S.A.S., A.A., G.W., and B.A.G. performed the statistical analyses. M.J., O.P., S.A.S., A.A., and B.A.G. designed the study and wrote the manuscript with the help of the coauthors J.K., S.A.K., C.B., S.G., E.K.-B., C. LaFougere, C. Laske, J.V., J.L., C.L.M., R.M., P.R.S., M.N.R., N.R.G.-R., S.S., B.G., J.M.R., J.M.N., J.C., A.M.G., T.L.S.B., J.C.M., R.J.B., G.W., A.M.F., and E.M.M.

Online content

Any methods, additional references, Nature Research reporting summaries, source data, statements of data availability and associated accession codes are available at https://doi.org/10.1038/s41591-018-0304-3.

Competing interests

A.M.G. has consulted for Cognition Therapeutics, Biogen, GlaxoSmithKline, Illumina, Eisai, AbbVie, and Pfizer and served on the Scientific Advisory Board for Denali Therapeutics. A.M.F. is a member of the Scientific Advisory Boards for AbbVie, Genentech and Roche Diagnostics and provides consultation for Araclon/Grifols and DiamiR.

Extended data is available for this paper at https://doi.org/10.1038/s41591-018-0304-3.

Supplementary information is available for this paper at https://doi.org/10.1038/s41591-018-0304-3.

Publisher's note: Springer Nature remains neutral with regard to jurisdictional claims in published maps and institutional affiliations.

Data availability

Data that support the findings of this study are available from DIAN at https://dian.wustl.edu/our-research/observational-study/dian-observational-study-investigator-resources/.

In most neurodegenerative diseases, brain changes manifest many years before clinical symptoms become apparent. In Alzheimer's disease, presymptomatic changes in the brain include cortical thinning and neuropathological depositions containing amyloid-β and tau. These pathological changes can be assessed by magnetic resonance imaging (MRI), positron-emission tomography (PET), and measurement of amyloid-β and tau protein levels in the cerebrospinal fluid (CSF)[1–4]. However, CSF collection is invasive and imaging modalities are expensive; therefore, they are not well suited to routine clinical practice. Blood biomarkers for the presymptomatic phase of Alzheimer's disease are largely lacking, although recent progress in the analysis of amyloid-β, tau, and neurofilament light chain (NfL) in the blood have been reported[5–10].

NfL is a component of the axonal cytoskeleton and is primarily expressed in large-caliber myelinated axons[11,12]. Changes of NfL in bodily fluids have been linked to brain damage and brain atrophy in mouse models and multiple neurological disorders including proteopathic neurodegenerative diseases[11,13–16]. Advancements in NfL measurements have revealed tight correlations between NfL in the CSF and blood and have sparked interest in an NfL blood-based biomarker that monitors neurodegeneration and disease progression. However, longitudinal analyses are largely missing and the importance of NfL as a molecular biomarker for the presymptomatic phase of neurodegenerative diseases remains unclear[6,9,17].

We made use of the Dominantly Inherited Alzheimer Network (DIAN)[18] data and biospecimens to study NfL changes in the CSF and blood of presymptomatic and symptomatic Alzheimer's disease. DIAN participants are members of families carrying highly penetrant autosomal-dominant mutations in the genes encoding the amyloid beta precursor protein (*APP*) or presenilin 1 (*PSEN1*) or 2 (*PSEN2*)[19]. Family members who do not carry the mutations serve as controls. Since the age of symptom onset tends to be consistent for a given mutation, it is possible to calculate for participants an estimated years to symptom onset (EYO) from the known onset of individuals with the same mutation[20].

We used the single-molecule array immunoassay technology to measure NfL in the CSF and blood serum of DIAN participants at their baseline (initial) visit (mutation carriers, $n = 243$; non-carriers, $n = 162$) (see Supplementary Table 1 for participant characteristics). Multivariate linear mixed effects models (LMEMs) served to assess the earliest point in the disease when NfL starts to increase in mutation carriers in relation to non-carriers (Fig. 1a,b). Results revealed that NfL in the CSF was significantly increased between mutation carriers and non-carriers at −6.8 EYO (Fig. 1a, Extended Data Fig. 1a). Almost identically, serum NfL was also increased at −6.8 EYO (Fig. 1b; Extended Data Fig. 1b). Consistent with our earlier work[13] CSF and serum NfL levels were tightly associated (Fig. 1c,d). No differences in CSF or serum NfL levels between the three familial Alzheimer's disease mutations were found (Extended Data Fig. 2).

Given the strong association between serum and CSF NfL, and the obvious advantage of a non-invasive disease blood biomarker[21], we chose to focus on serum NfL for subsequent longitudinal analyses. From the 405 participants with baseline serum, 196 returned for at least 1 and maximally 5 follow-up visits, with a mean number of 2.5 visits and a median

observation time of 3 years from the baseline visit (see Supplementary Table 2 for the longitudinal characteristics of participants).

Overall, the longitudinal analysis of serum NfL confirmed the cross-sectional findings (Fig. 2a). Using LMEMs we calculated the slope of NfL change per year for each participant. As with cross-sectional values, the NfL rates of change were significantly elevated in mutation carriers relative to non-carriers. Strikingly, however, the first EYO point where this increase became significant was at − 16.2 years (Fig. 2b; see also Extended Data Fig. 3), which is almost a decade earlier than the cross-sectional baseline estimates (−6.8 EYO, see earlier). Consistent with this earlier separation of mutation carriers and non-carriers using longitudinal measurements, the rate of change could distinguish presymptomatic mutation carriers from non-carriers more accurately compared to base-line serum NfL using receiver operating characteristics analysis (Extended Data Fig. 4).

Next, we subdivided mutation carriers into three groups: presymptomatic mutation carriers (individuals who scored 0 on the Clinical Dementia Rating (CDR) scale across all visits); converters (CDR = 0 at baseline and CDR > 0 at subsequent visits); and symptomatic mutation carriers (CDR > 0 across all visits). Then we compared the rate of change in serum NfL across these groups. Analyses revealed that the rate of change in serum NfL peaked in the converter group with no further increase in the symptomatic carriers (Fig. 2c). Interestingly, flattening or even U-shaped curves have also been observed in longitudinal studies for CSF biomarkers in dominant and sporadic AD[22,23].

No differences in NfL rate of change were found between mutations in *APP*, *PSEN1*, and *PSEN2* (Extended Data Fig. 5a). To analyze whether the NfL rate of change was associated with the aggressiveness of individual mutations or EYO, we analyzed how far away the NfL rate of change of each mutation carrier was from the median value from the model estimates at that individual's EYO (Extended Data Fig. 5b). Although we did not find any significant differences, it is possible that differences become apparent when the number of individuals and longitudinal data points increase.

To study if brain changes are coupled with changes in serum NfL, regression analysis between NfL rates of change and rates of change in brain imaging modalities were performed. We focused on the precuneus since previous analyses have shown this area to be most sensitive to Alzheimer's disease progression[2,24]. NfL rates of change in serum and rates of precuneus cortical thinning were significantly associated in symptomatic mutation carriers with a trend toward significance in presymptomatic mutation carriers (Fig. 3a). The rate of change in serum NfL and the rate of change in precuneus glucose metabolism (^{18}F-fluorodeoxyglucose (18F-FDG) PET) were significantly associated in symptomatic mutation carriers but not in presymptomatic mutation carriers (Fig. 3b). Although there was a positive relationship between NfL rate of change and the rate of change in precuneus amyloid-β deposition (amyloid-β-PET), the association did not reach significance (Fig. 3c). These results indicate that NfL changes in the blood most closely reflect cortical thinning and support the view that serum NfL is primarily a marker of neurodegeneration.

To examine the utility of serum NfL for predicting subsequent neurodegeneration and clinical symptoms, we performed a (retrospective) pseudo-predictive analysis to ask whether baseline serum NfL levels were predictive of subsequent cortical thinning (Fig. 4a). In addition, we assessed the predictability of baseline serum NfL for detecting change in two cognitive parameters, namely the Mini–Mental State Examination (MMSE) and the Logical Memory test (Fig. 4b,c). Indeed, baseline NfL was highly predictive of future annualized cortical thinning, for both presymptomatic and symptomatic mutation carriers, at subsequent visits (Fig. 4a) and was also predicative for a decrease in MMSE and Logical Memory scores (Fig. 4b,c).

To examine whether serum NfL is also predictive in a truly prospective design, the first 39 mutation carriers returning for follow-up visits after the last serum collection were included in the analysis. (The median time between last serum collection and subsequent visit was 2.1 years.) This prospective analysis allowed us to use the serum NfL rate of change for the prediction of further cortical thinning and cognitive changes (from the last visit with serum collection to the follow-up visit). Despite the small sample size, significant (predictive) associations were found between serum NfL rate of change and cortical thinning as well as MMSE and Logical Memory test (Fig. 4d–f).

Cross-sectional and longitudinal data analyses of DIAN and other large Alzheimer's disease cohorts have demonstrated that the pathological processes in Alzheimer's disease begin more than two decades before the onset of clinical symptoms. The accumulation of amyloid-β in the brain (estimated 15–20 years before clinical onset) is followed by declines in cortical metabolism (estimated 10–15 years before clinical onset) and brain atrophy (5–10 years before clinical onset)[1,2,22,25]. Thus, it is generally agreed that therapeutic interventions should start as early as possible making disease bio-markers of the presymptomatic phase of utmost importance[4,26]. The present results suggest that NfL levels in the blood may serve as such a biomarker to monitor neurodegeneration and disease progression already in presymptomatic Alzheimer's disease.

The strong association between NfL levels in the CSF and blood indicates that NfL changes in the blood reflect changes in the brain, a finding also reported for other neurodegenerative diseases including sporadic Alzheimer's disease[6,13,27,28]. In the present study serum was analyzed but similar levels and tight correlations have also been reported for NfL in the plasma[13,27]. The antigen detected with the (ultrasensitive) immunoassay used in this study is presumably a short and stable fragment (~10 kD) of the core domain of NfL[15,29]. Such a stable fragment appears well suited as a blood biomarker for monitoring a slow neurodegenerative process in the brain.

Using serial NfL measurements we found that the NfL annual rate of change can distinguish non-carriers and mutation carriers as early as 16 years before the estimated symptom onset. This is almost a decade earlier than when using absolute NfL levels measured at a single time point. Consistently, previous studies reported only non-significant or barely significant increases in absolute NfL in the blood in presymptomatic or even mildly cognitive impaired Alzheimer's disease patients[6,9,13]. In symptomatic Alzheimer's disease, our results suggest that the NfL rate of change reaches a plateau, whereas absolute NfL levels continue to

increase. Increased absolute NfL levels in the blood in the symptomatic disease phase is consistent with similar observations in progressive supranuclear palsy[28], Huntington's disease[30], and multiple sclerosis[14].

The very early changes of NfL in the blood may appear surprising in light of the reported overall brain atrophy only 5–10 years before symptom onset. However, atrophy of individual cortical regions occurs earlier[1,2,22,25]. In fact, precuneus thinning was also detected around 16 years before symptom onset2, suggesting that NfL changes are sensitive enough to pick up such early regional brain atrophy. The association between NfL and cortical thinning, rather than amyloid-β deposition, is in line with cerebral amyloid-β aggregation being a trigger of subsequent neurodegeneration that, however, become independent of each other at later disease stages[31]. The relationship of NfL to tau in bodily fluids needs further work. In the DIAN cohort, the increase of tau in the CSF (absolute levels, cross-sectional) occurs as early as 15 years before the estimated age of symptom onset[32], which is much earlier than the increase of base-line NfL in the CSF.

While an increase of NfL levels is not specific for Alzheimer's disease, the present findings are relevant for understanding Alzheimer's disease progression and highlight their utility as a marker in clinical trials. In presymptomatic Alzheimer's disease, the greater the NfL rate of change, the closer an individual is to converting to symptomatic Alzheimer's disease, a finding also reported for cortical atrophy[2,33]. This suggests that longitudinal measures of NfL in the serum are a reliable, relatively cheap, and fast readout of neurodegeneration in the brain with comparable diagnostic value to neuroimaging but without the regional resolution.

Although our prospective predication analysis was not adequately powered to demonstrate that NfL rate of change is indeed a better predictor of disease progression (neurodegeneration and cognitive decline) than absolute NfL values, our observations suggest that this is the case in presymptomatic Alzheimer's disease, while absolute NfL levels are better predictors in the symptomatic phase. Absolute NfL levels have been successfully used to predict brain volume changes in (symptomatic) multiple sclerosis[14] and clinical outcome in traumatic brain injury[34]. In a recent study with Huntington's disease patients, NfL blood levels were predictive of disease onset within three years[30], but NfL rate of change was not assessed.

The current study design with the 2–3 years interval between participant assessments did not allow us to determine the relationship between the time over which the NfL rate of change was calculated and its clinical predictability. However, the latter appears important to advance the NfL rate of change as a biomarker. Future analyses should also assess more accurately the disease period at which the NfL rate of change is a better predictor of neurodegeneration and cognitive decline than absolute NfL. Finally, it is important to translate our findings to sporadic Alzheimer's disease and other cerebral proteopathies[13,35]. Studies have indicated that the pathogenesis of familial and sporadic Alzheimer's disease are very similar and share similar pathophysiology and progression[36–39]. However, sporadic Alzheimer's disease patients are typically older and have more comorbidities, which in turn may influence NfL levels in the blood. The latter is however a further argument that absolute

NfL levels may be less useful for prediction in early disease stages compared to the NfL rate of change.

Methods

Participants.

Participants at 50% risk of carrying an autosomal-dominant Alzheimer's disease mutation in one of three genes (*APP, PSEN1, PSEN2*) were enrolled in the DIAN observational study (National Institute on Aging grant no. U19 AG032438; dian.wustl.edu; clinical trial no. NCT00869817)[18]. DIAN participants are assessed at baseline and subsequent follow-up visits (annually to every third year). Assessment included collection of body fluids (CSF, blood), clinical testing (CDR), neuropsychological testing (including MMSE (raw scores) and the Logical Memory subtest of the Wechsler Memory Scale-Revised (story A), raw scores for immediate and delayed recall), and imaging modalities (MRI, PET with Pittsburgh Compound B (PiB-PET), and ^{18}F-FDG) as described in earlier publications[1,2,40–42.] The institutional review board at Washington University in St. Louis provided supervisory review and human studies approval. Participants or their caregivers provided informed consent in accordance with their local institutional review boards. NfL analysis in the DIAN cohort was approved by the ethics committee at the medical faculty of the University of Tübingen, Germany (project number 718/2014BO2). The detailed number of participants (mutation carriers, non-carriers) for baseline and longitudinal measurements are given in Supplementary Tables 1 and 2 and the legends of Figs. 2, 3, and 4.

Clinical assessment and EYO.

The presence of dementia (symptoms) was assessed using the CDR[41]. Clinical evaluators were blinded to each participant's mutation status. For every visit a participant's EYO was calculated based on the participant's age at the visit relative to their 'mutation-specific' expected age at dementia onset. The mutation-specific expected age of dementia onset was computed by averaging the reported age of dementia onset across individuals with the same specific mutation[20]. If the mutation-specific expected age at dementia onset was unknown, the EYO was calculated from the age at which parental cognitive decline began. The parental age of clinical symptom onset was determined by a semi-structured interview with the use of all available historical data. The EYO was calculated identically for both mutation carriers and non-carriers. Mutation status was determined using PCR-based amplification of the appropriate exon followed by Sanger sequencing[1].

NfL measurements in the CSF and blood.

Fluids were collected in the morning under fasting conditions by venipuncture using a 21 gauge (G) butterfly needle and red top plain Vacutainer tubes (Becton, Dickinson and Company). After blood collection the tubes were left upside at room temperature for 30 min to allow clotting. After clotting, tubes were centrifuged at 2,000*g* for 15 min at room temperature. Serum was taken with a disposable, non-sterile transfer pipette into a single transfer tube (SARSTEDT AG & Co. KG) and immediately frozen on dry ice. After venipuncture, CSF was collected by gravity drip into two 13 ml polypropylene tubes using standard lumbar puncture procedures (L4-L5) with an atraumatic Sprotte spinal needle (22

G). As with serum, CSF was flash-frozen upright on dry ice. Samples collected in the United States were shipped overnight on dry ice to the DIAN biomarker core laboratory at Washington University, whereas samples collected at non-United States sites were stored at −80 °C and shipped quarterly on dry ice to Washington University. At the core laboratory the frozen samples were subsequently thawed, combined into a single polypropylene tube of serum or CSF, and aliquoted (300 or 500 μl) into polypropylene Corning microcentrifuge tubes (Thermo Fisher Scientific), after which they were again flash-frozen on dry ice and stored at −80 °C. For the current study, all available DIAN serum samples (data freeze 11) were shipped to the DIAN site in Tübingen. CSF samples (data freeze 9) were shipped to the DIAN site in Munich first and used for another analysis before being shipped to the DIAN site in Tübingen. Thus, CSF samples had one additional freeze–thaw cycle in Munich; however, prior work has indicated no significant effect of up to four freeze–thaw cycles on NfL in CSF[43].

CSF and serum NfL measurements were performed using a highly sensitive single-molecule array assay using the capture monoclonal antibody 47:3 and the biotinylated detection antibody 2:1 (UmanDiagnostics AB)[44]. The samples were measured in duplicate on a Simoa HD-1 platform (Quanterix) using a two-step neat assay. Serum samples were measured at 1:4 and CSF at 1:10 dilution (Tris-buffered saline, 0.1% Tween 20, 1% non-fat milk powder, HeteroBlock (300 ug ml^{-1}; Omega Biologicals)). Batch-prepared calibrators (bovine lyophilized NfL) ranging from 0 to 10,000 pg ml^{-1} were stored at −80 °C (Uman Diagnostics AB). All samples were measured blinded. For serum, the mean intra-assay coefficient of variation of duplicate determinations for concentration was 4.2%. In the CSF, the mean intra-assay coefficient of variation was 3.7%. Inter-assay variability was evaluated with three native serum samples and three native CSF samples. The inter-assay coefficients of variation for serum were 7.7% (mean concentration 13.3 pg ml^{-1}), 2.9% (30.9 pg ml^{-1}), and 3.7% (269.9 pg ml^{-1}). In the CSF, the interassay coefficients of variation were 2.4% (445.4 pg ml^{-1}), 12.2% (1486.3 pg ml^{-1}), and 13.3% (14,049.0 pg ml^{-1}). Note that the concentrations (pg ml^{-1}) are calculated from the full-length NfL calibrator and thus may overestimate the concentration of an NfL fragment in the blood.

Imaging.

MRI was performed at the different DIAN sites on 3T scanners using the Alzheimer's Disease Neuroimaging Initiative (ADNI) protocol. T1-weighted images (1.1 × 1.1 × 1.2 mm^3 voxels) were acquired for all participants. The ADNI Imaging Core screened images for artifacts and protocol compliance. FreeSurfer version 5.3 was used to perform volumetric segmentation and cortical surface reconstruction to define subcortical and cortical regions of interest (ROIs). Members of the DIAN Imaging Core examined each segmentation and edited them as needed. Cortical thickness measures were averaged across hemispheres. Since the precuneus region has been shown to be most sensitive to Alzheimer's disease pathophysiology in autosomal-dominant Alzheimer's disease[2,24], we focused our analyses on this region a priori.

Amyloid-β-PET imaging was done using a bolus injection of ^{11}C-PiB. Acquisition consisted of a 70-min scan starting at injection or a 30-min scan beginning 40 min after injection. Data

in the common 40–70 min time frame were converted to regional standardized uptake value ratios (SUVRs) relative to the cerebellar gray matter using FreeSurfer-derived ROIs (PET Unified Pipeline, https://github.com/ysu001/PUP). Metabolic imaging was done with ^{18}F-FDG PET with a 30 min dynamic acquisition beginning 30 min after injection. Data from the 40–60 min time frame were converted to SUVRs relative to cerebellar gray matter. The ADNI Imaging Core verified that the PET images were acquired using the established protocol and free of substantial artifacts. All PET data were partial volume-corrected using a regional spread function technique. Scanner-specific spatial filters were applied to achieve a common resolution (8 mm) across PET scanners. MRI and PET data acquisition and processing has been described in detail in previous studies[1,2,24]. Again, for the present analyses, we averaged SUVR values from the bilateral precuneus ROIs defined on the MRI.

Statistical analysis.

Relating baseline CSF and serum NfL.—The relationship between baseline CSF and serum NfL was determined by using LMEMs implemented in R version 3.4.2 and RStudio version 1.1.453 using the package lme4, including a random intercept term for family and fixed effect for baseline age, sex, and baseline CSF NfL, with baseline serum NfL as the dependent variable. Separate models were fitted for non-carriers and mutation carriers. Baseline CSF and serum NfL values were log-transformed (due to non-normal distribution) before being entered into the model. See also Supplementary statistical analysis.

Baseline CSF and serum NfL as a function of EYO.—The relationship between EYO and baseline CSF and serum NfL values was estimated using LMEMs. As previously done, to account for potential non-linear effects, EYO was modeled as a restricted cubic spline with knots at the 0.10, 0.50, and 0.90 quantiles[2]. The LMEMs for the baseline NfL values (CSF or serum) included: fixed effects for mutation status; the linear EYO component; the cubic EYO component; the linear EYO by mutation status interaction; the cubic EYO by mutation status interaction; and a random intercept for family. Model parameters were estimated using an open source package for Hamiltonian Markov chain Monte Carlo analyses, Stan (http://mc-stan.org/)[45,46], implemented using R. This resampling approach leads to a distribution of parameter estimates across iterations. From this distribution it is possible to estimate the 99% credible intervals of the model fits at every EYO for non-carriers, mutation carriers, and the distribution of the difference between non-carriers and mutation carriers. The first EYO where groups (non-carriers and mutation carriers) differed was determined to be the first point where the 99% credible intervals around the differences distribution between non-carriers and mutation carriers did not overlap 0. See also Supplementary statistical analysis.

Calculating the rate of change in biomarkers.—Longitudinal data was modeled using LMEMs. LMEMs are a powerful approach to account for the covariance structure introduced by serial measurements and are ideal to deal with imperfect timing or an unbalanced number of data points. The rate of change in log-transformed serum NfL for each individual was modeled using an LMEM with fixed effects of time from baseline (in years), mutation status, a time from baseline by mutation status interaction, and a random intercept for family, as well as random slope and intercept terms for each participant. The

rate of NfL change for each individual was extracted from the model estimates for subsequent analyses. This model was also used for generating the rate of change for cortical thickness,18F-FDG PET, and PiB-PET, for each individual (for plotting purposes). See also Supplementary statistical analysis.

Longitudinal serum NfL as a function of EYO and cognitive status.—As with the cross-sectional estimates, the relationship between EYO and rate of change in serum NfL was estimated using an LMEM in Stan. The EYO was modeled as a restricted cubic spline with knots at the 0.10, 0.50, and 0.90 quantiles. The LMEM model for the rate of change in serum NfL included: fixed effects for mutation status; the linear EYO component; the cubic EYO component; the linear EYO by mutation status interaction; the cubic EYO by mutation status interaction; and a random intercept for family. Model parameters were estimated using Stan. Again, this resampling approach leads to a distribution of parameters estimates across iterations, resulting in 99% credible intervals of the model fits at every EYO for non-carriers, mutation carriers, and the distribution of the difference between non-carriers and mutation carriers. The first EYO where groups (non-carriers and mutation carriers) differed was determined to be the first point where the 99% credible intervals around the differences distribution between non-carriers and mutation carriers did not overlap 0.

To determine whether the extracted rate of change in serum NfL was significantly different across mutation status and cognitive status we categorized mutation carriers based on cognitive status, where presymptomatic mutation carriers were individuals who scored as CDR = 0 across all visits ($n = 65$), converters were mutation carriers who scored as CDR = 0 at baseline and CDR > 0 at subsequent visits ($n = 13$), and symptomatic mutation carriers were individuals who scored as CDR > 0 across all visits ($n = 55$). We used LMEMs, including a random intercept for family and fixed effects for baseline age, sex, and group (that is, non-carriers, presymptomatic mutation carriers, converters, or symptomatic mutation carriers), where group was the term of interest, and the extracted rate of change in serum NfL was the dependent variable. Models were computed using lme4 in R. See also Supplementary statistical analysis.

Association between expected age of onset and deviation from the EYO-adjusted median rate of change in NfL.—We tested the hypothesis of whether individuals who have an earlier expected age of onset (for example, age of onset of 30 years old versus 55 years old) have an accelerated NfL rate of change. First, to determine if a participant deviated from its expected NfL rate of change, given its baseline EYO, we calculated the median rate of change in NfL at each EYO, generated from model estimates (for the calculation, see ‘Baseline CSF and serum NfL and longitudinal NfL as a function of EYO’ in the Supplementary statistical analysis; for the depiction of median values, see the red line in Fig. 2b). We then took each participant’s extracted NfL rate of change and subtracted the median value corresponding to its baseline EYO. This resulting value represented the deviation from the expected value, whereby a positive value on this deviation measure indicates that an individual has a higher rate of change in serum NfL (that is, worse) than would be expected given their EYO. Conversely, a negative value on this deviation measure indicates that an individual has a lower rate of change in serum NfL (that

is, better) than would be expected given their EYO. Next, to investigate if there was a relationship between individuals with the higher deviation measure and earlier expected age of onset, we grouped individuals by their expected age of onset (determined by their specific mutation type, grouped as age of onset 20–39, 40–49, 50–59, and 60+). See also Supplementary statistical analysis.

Relating NfL rate of change to imaging rate of change.—The longitudinal relationship between the rate of change in serum NfL and concurrent rate of change in cortical thickness, metabolism, or amyloid-β accumulation was determined within each group of interest (that is, non-carriers, presymptomatic mutation carriers, and symptomatic mutation carriers). Therefore, separate models were run for each non-carrier, presymptomatic mutation carrier, and symptomatic mutation carrier groups. The dependent term for each model was an imaging biomarker with fixed effect terms for baseline age, sex, time from baseline, extracted rate of change in serum NfL, and interaction between time from baseline and rate of change in serum NfL. Models contained random slope and intercept terms for participants and random intercepts for family. The primary term of interest was the interaction between the rate of change in serum NfL and the time from baseline term. Models were fitted using lme4 in R.

To determine whether the relationship between groups was different, a model for each imaging modality containing all groups was run. Each model was fitted containing fixed effect terms for baseline age, sex, time from baseline, extracted rate of change in serum NfL, group (non-carriers, presymptomatic mutation carriers, or symptomatic mutation carriers), and two- and three-way interaction between time from baseline, rate of change in serum NfL, and group. Converters were included as part of the symptomatic mutation carrier group. The models also included random slope and intercept terms for the participants and random intercepts for family. The dependent variables were the longitudinal measures for cortical thickness, glucose metabolism, or amyloid-β deposition in the precuneus ROI. See also Supplementary statistical analysis.

Serum NfL at baseline predicts annual changes in cortical thickness and cognition.—To examine whether baseline serum NfL could predict subsequent changes in cortical thickness and cognition in mutation carriers we fitted LMEMs with random slope and intercept terms for participants, random intercepts for family, and fixed effect terms for baseline age, sex, time, log-transformed baseline serum NfL, and an interaction between time and baseline serum NfL. The interaction term was the term of interest. The dependent terms entered into the models were longitudinal precuneus cortical thickness measurements, MMSE scores, and Logical Memory test scores. If significant, an association of baseline serum NfL with rate of change in cortical thickness or cognition was assumed. See also Supplementary statistical analysis.

Prospective prediction of cortical thickness and cognition by serum NfL rate of change.—To determine whether the rate of change in serum NfL could predict subsequent changes in cortical thickness or cognition, we conducted a truly prospective study, whereby after longitudinal serum collection for NfL, we collected additional imaging and neuropsychological data on 39 mutation carriers. Twenty-eight individuals completed

additional imaging and neuropsychological testing, 9 completed only additional neuropsychological testing but no MRI, and 2 who completed an additional MRI but not neuropsychological testing. To determine the rate of change in cortical thickness and cognition (MMSE, Logical Memory test) between the imaging and cognitive assessment concurrent to the participant's last blood draw and follow-up session, we fitted an LMEM for each participant, where the dependent variable was the imaging or cognitive variable of interest at last serum visit and follow-up visit and the independent variable was the time between visits. Models were run in R. We then used this rate of change for cortical thickness or cognition as the dependent variable in an LMEM, which included fixed effects for age, sex, and the rate of change in serum NfL, and a random intercept term for family. The term of interest was the serum NfL rate of change. Models were fitted using lme4 in R. See also Supplementary statistical analysis.

Further statistical analyses and models.—The unstandardized regression coefficients (*B*), standard error of the mean (s.e.m.), and *P* values from the LMEMs and linear regression models are reported in the figure legends. The statistical analyses mentioned in the figure legends of Extended Data Figs. 2–4 and Supplementary Tables 1 and 2 were conducted using the JMP software, version 13.0 (SAS Institute Inc.). For the analysis of Extended Data Fig. 3c a regression model was created, which approximates the changes of non-carriers and mutation carriers. The model uses the rate of change of log serum NfL over EYO. For non-carriers a slightly increasing line over the entire time period was created representing the NfL increase over age. For mutation carriers the same development was taken for the very early years until a bifurcation point indicating the divergence of non-carriers and mutation carriers. From this point on, mutation carriers were shown with a rising slope up to a break of slope, when the line came to a parallel increase as non-carriers. This model uses one common slope at the very beginning, one bifurcation point, and one shift leading to two parallel slopes after symptom onset. See also Supplementary statistical analysis.

Reporting Summary.

Further information on research design is available in the Nature Research Reporting Summary linked to this article.

Supplementary Material

Refer to Web version on PubMed Central for supplementary material.

Extended Data

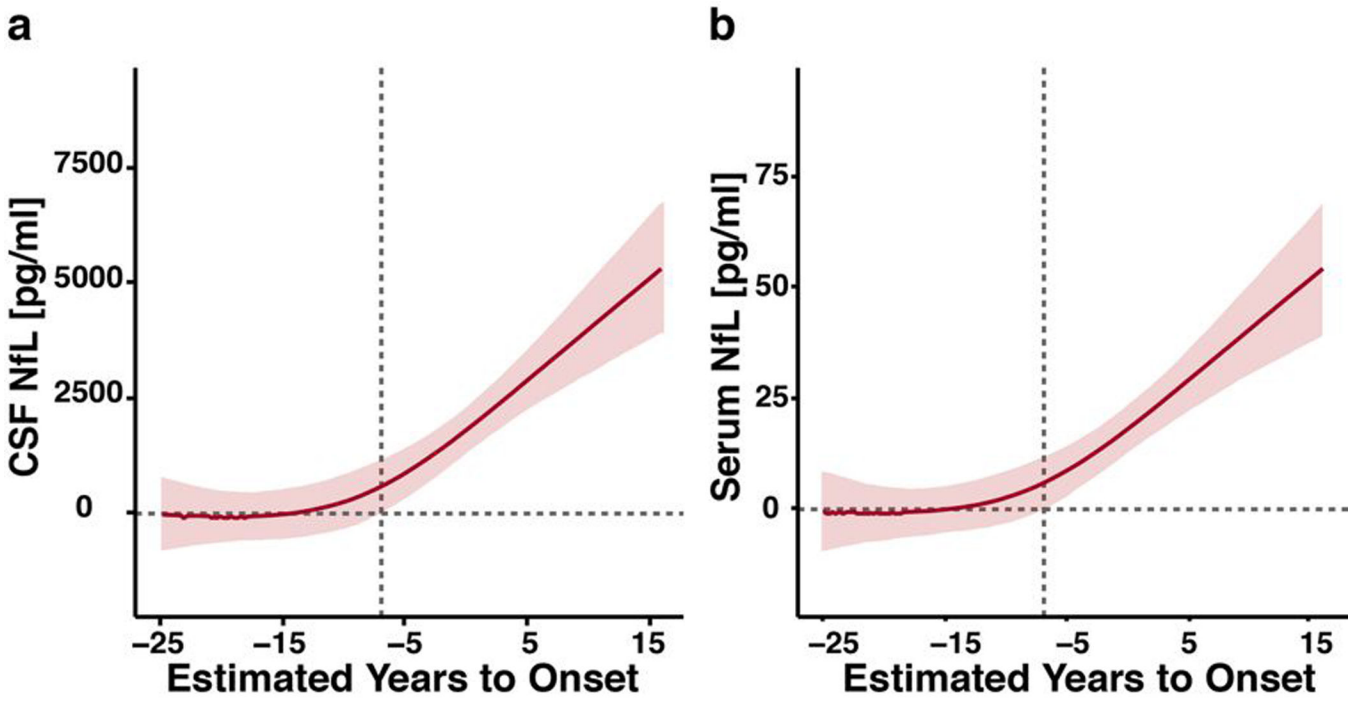

Extended Data Fig. 1 |. Difference distribution curve for baseline (cross-sectional) CSF and serum NfL levels in mutation carriers and non-carriers.

a,**b**, Difference of posterior distribution for baseline CSF NfL (n = 187) (**a**) and baseline serum NfL (n = 405) (**b**) as a function of EYO. The solid red lines depict the median of the difference distribution; the shaded area represents the 99% equal-tailed credible intervals. EYO was considered statistically significant if the 99% equal-tailed credible intervals of the posterior distribution did not overlap 0 (6.8 years before EYO for both baseline CSF and serum NfL). For the absolute values of baseline CSF and serum NfL, see Fig. 1a,b.

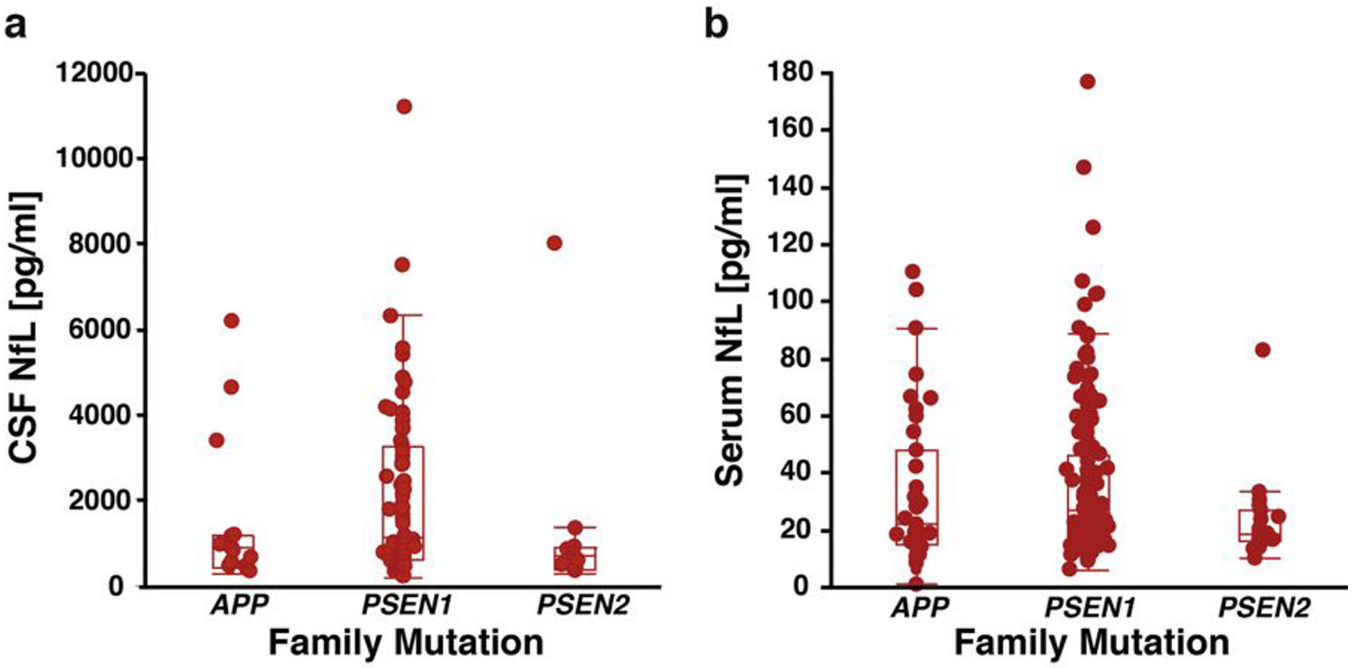

Extended Data Fig. 2 |. No difference in baseline CSF and serum NfL levels among *APP*, *PSEN1*, and *PSEN2* mutation carriers.

a, Two-tailed pairwise Student's *t*-test comparisons of CSF NfL levels of carriers of a mutation in *APP* ($n = 14$), *PSEN1* ($n = 82$), or *PSEN2* ($n = 11$). **b**, Same analysis, using a two-tailed pairwise Student's *t*-test for the serum NfL of carriers of a mutation in *APP* ($n = 39$), *PSEN1* ($n = 185$), or *PSEN2* ($n = 19$). No differences in log(CSF NfL) or log(serum NfL) were found between the groups ($F(2, 104) = 1.8108$, $P = 0.1686$ and $F(2, 240) = 1.9205$, $P = 0.1488$, respectively). Similarly, no differences were found by two-tailed pairwise Student's *t*-test when age and disease status (presymptomatic, symptomatic) were treated as covariates. The boxes map to the median, 25th and 75th quintiles, and the whiskers extend to the 1.5 × IQR.

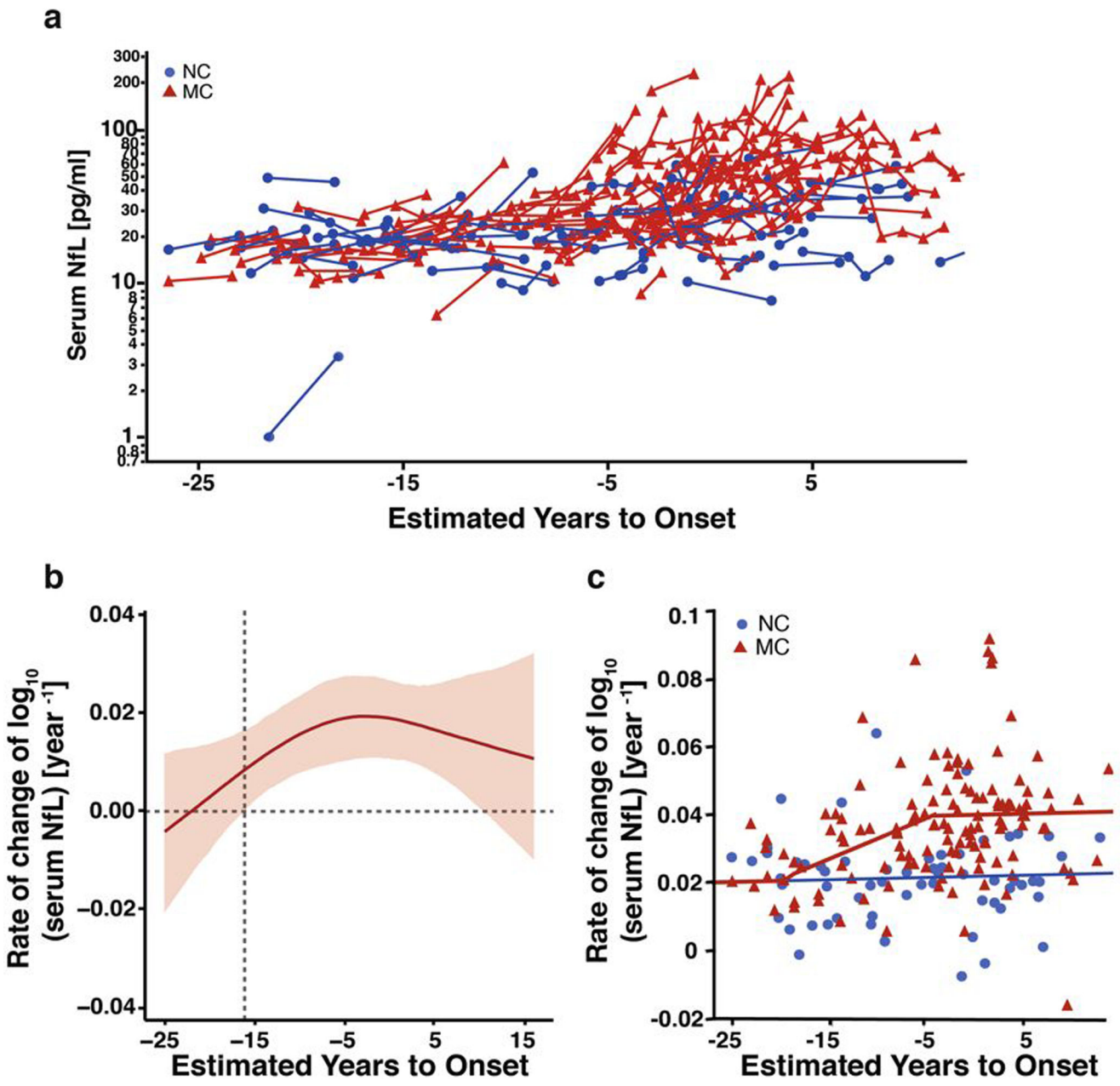

Extended Data Fig. 3 |. Longitudinal serum NfL and bifurcation of mutation carriers from non-carriers.

a, Spaghetti plot showing longitudinal serum NfL for non-carriers (NC, $n = 63$, blue) and mutation carriers (MC, $n = 133$, red) as a function of EYO. These are the same data as in Fig. 2a but with a logarithmic scale on the y axis to better appreciate the changes during the presymptomatic stage (for details, see Fig. 2a). **b**, Difference of posterior distribution for serum NfL rate of change between mutation carriers and non-carriers, as a function of EYO ($n = 196$). The solid red line depicts the median of the difference distribution, and the shaded area represents the 99% equal-tailed credible intervals. EYO was considered statistically significant if the 99% equal-tailed credible intervals of the posterior distribution did not

overlap 0 (16.2 years before EYO). **c**, Individual estimated rate of change in serum NfL (same data as in Fig. 2b, $n = 63$ for non-carriers and $n = 133$ for mutation carriers). A regression analysis was performed with two breaks of slope (see Methods for calculation). With this model the first bifurcation point was found at −18.6 years before EYO, the second at −5.8 years before EYO.

	NC vs presymptomatic MC		NC vs symptomatic MC	
	Cross-sectional (Baseline value)	Longitudinal (Rate of change per year)	Cross-sectional (Baseline value)	Longitudinal (Rate of change per year)
ROC curve	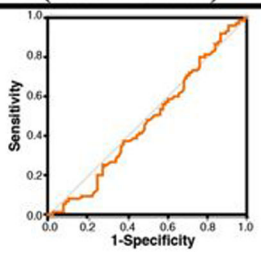	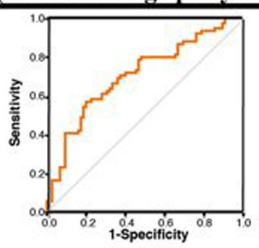	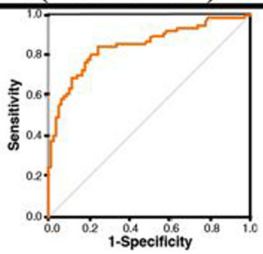	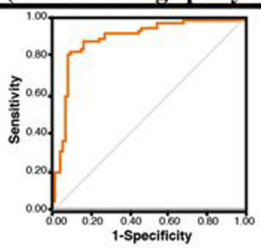
AUC	0.49	0.70	0.85	0.89
Specificity	14%	78%	75%	89%
Sensitivity	92%	58%	85%	82%
Cutoff value	37.4 pg/ml	0.027	27.9 pg/ml	0.033
n	Total=319 (NC=162, preMC=157)	Total=141 (NC=63,preMC=78)	Total=248 (NC=162, sMC=86)	Total=118 (NC=63, sMC=55)
p-value (χ^2)	0.6485	0.0002	<0.0001	<0.0001

Extended Data Fig. 4 |. Rate of change per year of serum NfL is a better parameter to distinguish presymptomatic and symptomatic mutation carriers from non-carriers compared to single cross-sectional serum NfL.

Receiver operating characteristic analysis for non-carriers (NC) versus presymptomatic mutation carriers (MC) and non-carriers versus symptomatic mutation carriers with cross-sectional (baseline serum NfL) and longitudinal (serum NfL rate of change per year) data. The true positive fraction (sensitivity) is on the *y* axis and the false positive fraction (1-specificity) on the *x* axis. The area under the curve (AUC, accuracy), as well as the cutoff value and χ^2 *P* value from the logistic regression are shown. The chance level of the area under the curve is 0.50. Converters (for rate of change, see Fig. 2c) were considered presymptomatic mutation carriers.

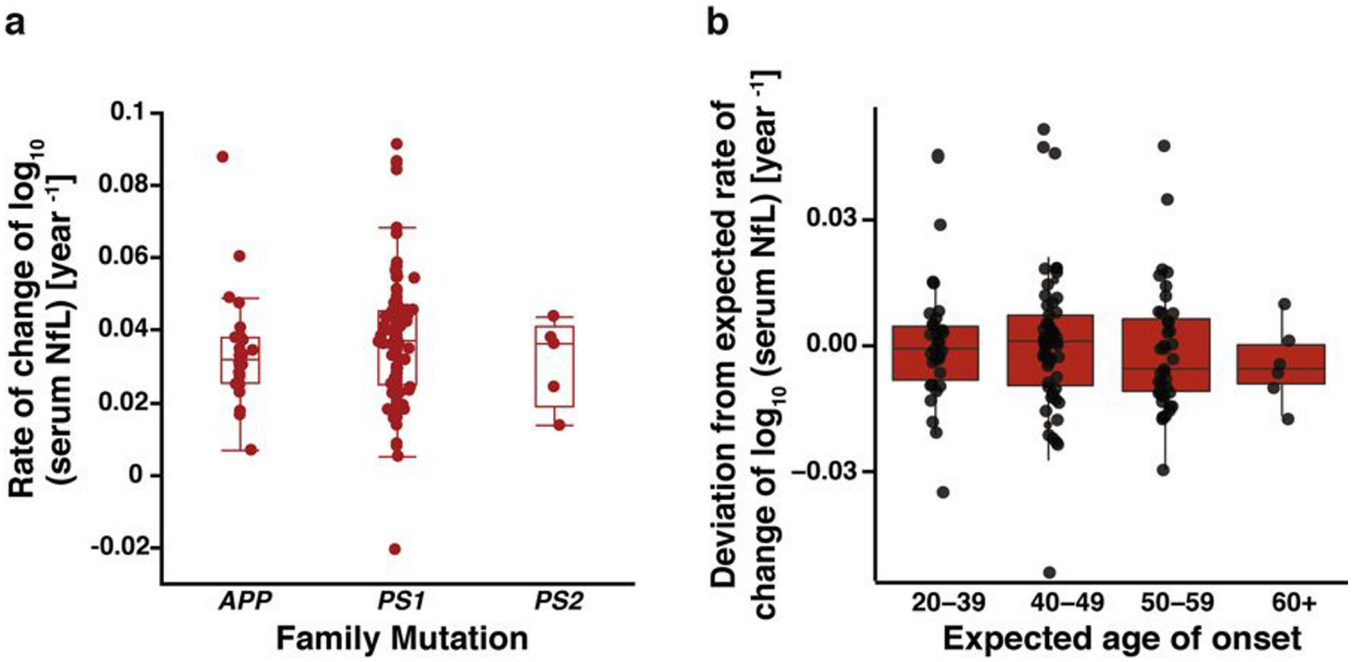

Extended Data Fig. 5 |. No difference in serum NfL rate of change among *APP*, *PSEN1*, and *PSEN2* mutation carriers and no association with estimated age of onset.

a, Using two-tailed pairwise Student's *t*-tests, no differences in the rate of change of log(serum NfL) (year^{-1}) levels among *APP* (n = 24), *PSEN1* (n = 104), and *PSEN2* (n = 5) mutation carriers ($F(2, 130) = 0.4678$, $P = 0.6274$) was found. Similarly, no differences were found when age and disease status (presymptomatic, symptomatic) were treated as covariates in a two-tailed pairwise Student's *t*-test. **b**, No difference between an individual's deviation from the EYO-adjusted median rate of change in NfL and their expected age of symptom onset using LMEMs. Individuals were grouped in 4 categories with expected symptom onset at 20–39 (n = 17), 40–49 (n = 54), 50–59 (n = 56), and over 60 years of age (n = 6); group comparisons, $P > 0.146$. See Methods for the calculations. The boxes map to the median, 25th and 75th quintiles, and the whiskers extend to the 1.5 × IQR.

Authors

Oliver Preische[1,2,21], Stephanie A. Schultz[3,21], Anja Apel[1,2,21], Jens Kuhle[4], Stephan A. Kaeser[1,2], Christian Barro[4], Susanne Gräber[1], Elke Kuder-Buletta[1], Christian LaFougere[1], Christoph Laske[1,2], Jonathan Vöglein[5,6], Johannes Levin[5,6], Colin L. Masters[7], Ralph Martins[8,9], Peter R. Schofield[10,11], Martin N. Rossor[12], Neill R. Graff-Radford[13], Stephen Salloway[14], Bernardino Ghetti[15], John M. Ringman[16], James M. Noble[17], Jasmeer Chhatwal[18], Alison M. Goate[19], Tammie L. S. Benzinger[3], John C. Morris[3], Randall J. Bateman[3], Guoqiao Wang[3], Anne M. Fagan[3], Eric M. McDade[3], Brian A. Gordon[3], Mathias Jucker[1,2,*], Alzheimer Network[20], Ricardo Allegri[22], Fatima Amtashar[23], Randall Bateman[23], Tammie Benzinger[23], Sarah Berman[24], Courtney Bodge[25], Susan Brandon[23], William Brooks[26], Jill Buck[27], Virginia Buckles[23], Sochenda Chea[28], Jasmeer Chhatwal[29], Patricio Chrem[22], Helena Chui[30], Jake Cinco[31], Jack Clifford[28], Carlos Cruchaga[23],

Mirelle D'Mello[26], Tamara Donahue[23], Jane Douglas[31], Noelia Edigo[22], Nilufer Erekin-Taner[28], Anne Fagan[23], Marty Farlow[27], Angela Farrar[23], Howard Feldman[32], Gigi Flynn[23], Nick Fox[31], Erin Franklin[23], Hisako Fujii[33], Cortaiga Gant[23], Samantha Gardener[34], Bernardino Ghetti[27], Alison Goate[35], Jill Goldman[36], Brian Gordon[23], Neill Graff-Radford[28], Julia Gray[23], Jenny Gurney[23], Jason Hassenstab[23], Mie Hirohara[37], David Holtzman[23], Russ Hornbeck[23], Siri Houeland DiBari[38], Takeshi Ikeuchi[39], Snezana Ikonomovic[24], Gina Jerome[23], Mathias Jucker[40], Celeste Karch[23], Kensaku Kasuga[39], Takeshi Kawarabayashi[37], William Klunk[24], Robert Koeppe[41], Elke Kuder-Buletta[40], Christoph Laske[40], Jae-Hong Lee[42], Johannes Levin[38], Daniel Marcus[23], Ralph Martins[34], Neal Scott Mason[43], Colin Masters[44], Denise Maue-Dreyfus[23], Eric McDade[23], Lucy Montoya[30], Hiroshi Mori[33], John Morris[23], Akem Nagamatsu[45], Katie Neimeyer[36], James Noble[36], Joanne Norton[23], Richard Perrin[23], Marc Raichle[23], John Ringman[30], Jee Hoon Roh[42], Stephen Salloway[25], Peter Schofield[26], Hiroyuki Shimada[33], Tomoyo Shiroto[37], Mikio Shoji[37], Wendy Sigurdson[23], Hamid Sohrabi[34], Paige Sparks[29], Kazushi Suzuki[45], Laura Swisher[23], Kevin Taddei[34], Jen Wang[35], Peter Wang[23], Mike Weiner[46], Mary Wolfsberger[23], Chengjie Xiong[23], and Xiong Xu[23]

Affiliations

[1]German Center for Neurodegenerative Diseases (DZNE), Tübingen, Germany. [2]Department of Cellular Neurology, Hertie Institute for Clinical Brain Research, and Department of Psychiatry and Psychotherapy, University of Tübingen, Tübingen, Germany. [3]Department of Neurology, Department of Radiology, and Division of Biostatistics, Washington University School of Medicine, St. Louis, MO, USA. [4]Neurologic Clinic and Policlinic, Departments of Medicine, Biomedicine and Clinical Research, University Hospital Basel, University of Basel, Basel, Switzerland. [5]German Center for Neurodegenerative Diseases (DZNE), Munich, Germany. [6]Department of Neurology, Ludwig-Maximilians-Universität München, Munich, Germany. [7]Neurodegeneration Division, The Florey Institute of Neuroscience and Mental Health, University of Melbourne, Parkville, Victoria, Australia. [8]School of Medical Health and Sciences, Edith Cowan University, Joondalup, Western Australia, Australia. [9]Department of Biomedical Sciences, Macquarie University, Sydney, New South Wales, Australia. [10]Neuroscience Research Australia, Randwick, New South Wales, Australia. [11]School of Medical Sciences, University of New South Wales, Sydney, New South Wales, Australia. [12]Dementia Research Centre, Department of Neurodegeneration, Queen Square Institute of Neurology, University College London, London, UK. [13]Department of Neurology, Mayo Clinic Jacksonville, Jacksonville, FL, USA. [14]Warren Alpert Medical School of Brown University, Providence, RI, USA. [15]Indiana Alzheimer Disease Center and Department of Pathology and Laboratory Medicine, Indiana University School of Medicine, Indianapolis, IN, USA. [16]Department of Neurology, Keck School of Medicine at USC, Los Angeles, CA, USA. [17]Taub Institute for Research on Alzheimer's Disease and the Aging Brain, Department of Neurology, Columbia University Medical Center, New York, NY, USA. [18]Department of Neurology,

Massachusetts General Hospital, Harvard Medical School, Boston, MA, USA. [19]Department of Neuroscience, Icahn School of Medicine at Mount Sinai, New York, NY, USA. [20]A full list of members and affiliations appears at the end of the paper. [21]These authors contributed equally: Oliver Preische, Stephanie A. Schultz, Anja Apel. [22]FLENI Institute of Neurological Research (Fundacion para la Lucha contra las Enfermedades Neurologicas de la Infancia), Buenos Aries, Argentina. [23]Washington University School of Medicine, St. Louis, MO, USA. [24]University of Pittsburgh, Pittsburgh, PA, USA. [25]Brown University-Butler Hospital, Providence, RI, USA. [26]Neuroscience Research Australia, Sydney, New South Wales, Australia. [27]Indiana University, Bloomington, IN, USA. [28]Mayo Clinic Jacksonville, Jacksonville, FL, USA. [29]Brigham and Women's Hospital–Massachusetts General Hospital, Boston, MA, USA. [30]University of Southern California, Los Angeles, CA, USA. [31]University College London, London, UK. [32]University of California San Diego, San Diego, CA, USA. [33]Osaka City University, Osaka, Japan. [34]Edith Cowan University, Perth, Western Australia, Australia. [35]Icahn School of Medicine at Mount Sinai, New York, NY, USA. [36]Columbia University, New York, NY, USA. [37]Hirosaki University, Aomori, Japan. [38]German Center for Neurodegenerative Diseases (DZNE), Munich, Germany. [39]Niigata University, Niigata, Japan. [40]German Center for Neurodegnerative Diseases (DZNE), Tubingen, Germany. [41]University of Michigan, Ann Arbor, MI, USA. [42]Asan Medical Center, Seoul, South Korea. [43]University of Pittsburgh Medical Center, Pittsburgh, PA, USA. [44]University of Melbourne, Melbourne, Victoria, Australia. [45]Tokyo University, Tokyo, Japan. [46]University of California San Francisco, San Francisco, CA, USA.

Acknowledgements

We would like to thank M. Staufenbiel and M. Eichner for support and helpful comments and C. Haass and M. Suarez (Munich) for experimental and logistic support. Data collection and sharing for this project was supported by DIAN (grant no. UF1AG032438) funded by the National Institute on Aging and the German Center for Neurodegenerative Diseases (DZNE). Additional support came from the National Institutes of Health-funded NINDS Center Core for Brain Imaging (grant no. P30NS098577), the National Science Foundation (grant no. DGE-1745038), National Institutes of Health (grant no. UL1TR001873 to J.M.N.), the Swiss National Science Foundation (grant no. 320030–160221 to J.K.), the National Institute for Health Research University College London Hospitals Biomedical Research Centre, and the MRC Dementias Platform UK (grant nos. MR/L023784/1 and MR/009076/1). We acknowledge the altruism of the participants and their families and input of the DIAN research and support staff at each of the participating sites for their contributions to this study.

References

1. Bateman RJ et al. Clinical and biomarker changes in dominantly inherited Alzheimer's disease. N. Engl. J. Med 367, 795–804 (2012). [PubMed: 22784036]
2. Gordon BA et al. Spatial patterns of neuroimaging biomarker change in individuals from families with autosomal dominant Alzheimer's disease: a longitudinal study. Lancet Neurol 17, 241–250 (2018). [PubMed: 29397305]
3. Jack CR, Jr. et al. NIA-AA Research Framework: toward a biological definition of Alzheimer's disease. Alzheimers Dement 14, 535–562 (2018). [PubMed: 29653606]
4. Sperling RA, Karlawish J & Johnson KA Preclinical Alzheimer disease: the challenges ahead. Nat. Rev. Neurol 9, 54–58 (2013). [PubMed: 23183885]

5. Fandos N et al. Plasma amyloid β 42/40 ratios as biomarkers for amyloid β cerebral deposition in cognitively normal individuals. Alzheimers Dement. (Amst) 8, 179–187 (2017). [PubMed: 28948206]
6. Mattsson N, Andreasson U, Zetterberg H & Blennow K Association of plasma neurofilament light with neurodegeneration in patients with Alzheimer disease. JAMA Neurol 74, 557–566 (2017). [PubMed: 28346578]
7. Nakamura A et al. High performance plasma amyloid-β biomarkers for Alzheimer's disease. Nature 554, 249–254 (2018). [PubMed: 29420472]
8. Ovod V et al. Amyloid β concentrations and stable isotope labeling kinetics of human plasma specific to central nervous system amyloidosis. Alzheimers Dement 13, 841–849 (2017). [PubMed: 28734653]
9. Weston PSJ et al. Serum neurofilament light in familial Alzheimer disease: a marker of early neurodegeneration. Neurology 89, 2167–2175 (2017). [PubMed: 29070659]
10. Mielke MM et al. Plasma phospho-tau181 increases with Alzheimer's disease clinical severity and is associated with tau- and amyloid-positron emission tomography. Alzheimers Dement 14, 989–997 (2018). [PubMed: 29626426]
11. Petzold A Neurofilament phosphoforms: surrogate markers for axonal injury, degeneration and loss. J. Neurol. Sci 233, 183–198 (2005). [PubMed: 15896809]
12. Schlaepfer WW & Lynch RG Immunofluorescence studies of neurofilaments in the rat and human peripheral and central nervous system. J. Cell Biol 74, 241–250 (1977). [PubMed: 326799]
13. Bacioglu M et al. Neurofilament light chain in blood and CSF as marker of disease progression in mouse models and in neurodegenerative diseases. Neuron 91, 56–66 (2016). [PubMed: 27292537]
14. Barro C et al. Serum neurofilament as a predictor of disease worsening and brain and spinal cord atrophy in multiple sclerosis. Brain 141, 2382–2391 (2018).
15. Brureau A et al. NF-L in cerebrospinal fluid and serum is a biomarker of neuronal damage in an inducible mouse model of neurodegeneration. Neurobiol. Dis 104, 73–84 (2017). [PubMed: 28392472]
16. Kuhle J et al. Serum neurofilament light chain in early relapsing remitting MS is increased and correlates with CSF levels and with MRI measures of disease severity. Mult. Scler 22, 1550–1559 (2016). [PubMed: 26754800]
17. Zhou W et al. Plasma neurofilament light chain levels in Alzheimer's disease. Neurosci. Lett 650, 60–64 (2017). [PubMed: 28428015]
18. Morris JC et al. Developing an international network for Alzheimer research: the Dominantly Inherited Alzheimer Network. Clin. Investig. (Lond) 2, 975–984 (2012).
19. Moulder KL et al. Dominantly Inherited Alzheimer Network: facilitating research and clinical trials. Alzheimers Res. Ther 5, 48 (2013). [PubMed: 24131566]
20. Ryman DC et al. Symptom onset in autosomal dominant Alzheimer disease: a systematic review and meta-analysis. Neurology 83, 253–260 (2014). [PubMed: 24928124]
21. Henriksen K et al. The future of blood-based biomarkers for Alzheimer's disease. Alzheimers Dement 10, 115–131 (2014). [PubMed: 23850333]
22. McDade E et al. Longitudinal cognitive and biomarker changes in dominantly inherited Alzheimer disease. Neurology 91, e1295–e1306 (2018). [PubMed: 30217935]
23. Sutphen CL et al. Longitudinal decreases in multiple cerebrospinal fluid biomarkers of neuronal injury in symptomatic late onset Alzheimer's disease. Alzheimers Dement 14, 869–879 (2018). [PubMed: 29580670]
24. Benzinger TLS et al. Regional variability of imaging biomarkers in autosomal dominant Alzheimer's disease. Proc. Natl Acad. Sci. USA 110, E4502–E4509 (2013). [PubMed: 24194552]
25. Burnham SC et al. Clinical and cognitive trajectories in cognitively healthy elderly individuals with suspected non-Alzheimer's disease pathophysiology (SNAP) or Alzheimer's disease pathology: a longitudinal study. Lancet Neurol 15, 1044–1053 (2016). [PubMed: 27450471]
26. Jack CR, Jr. & Holtzman DM Biomarker modeling of Alzheimer's disease. Neuron 80, 1347–1358 (2013). [PubMed: 24360540]

27. Lu CH et al. Neurofilament light chain: a prognostic biomarker in amyotrophic lateral sclerosis. Neurology 84, 2247–2257 (2015). [PubMed: 25934855]
28. Rojas JC et al. Plasma neurofilament light chain predicts progression in progressive supranuclear palsy. Ann. Clin. Transl. Neurol 3, 216–225 (2016). [PubMed: 27042681]
29. Norgren N, Karlsson JE, Rosengren L & Stigbrand T Monoclonal antibodies selective for low molecular weight neurofilaments. Hybrid. Hybridomics 21, 53–59 (2002). [PubMed: 11991817]
30. Byrne LM et al. Neurofilament light protein in blood as a potential biomarker of neurodegeneration in Huntington's disease: a retrospective cohort analysis. Lancet Neurol 16, 601–609 (2017). [PubMed: 28601473]
31. Karran E, Mercken M & De Strooper B The amyloid cascade hypothesis for Alzheimer's disease: an appraisal for the development of therapeutics. Nat. Rev. Drug Discov 10, 698–712 (2011). [PubMed: 21852788]
32. Fagan AM et al. Longitudinal change in CSF biomarkers in autosomal-dominant Alzheimer's disease. Sci. Transl. Med 6, 226ra230 (2014).
33. Kinnunen KM et al. Presymptomatic atrophy in autosomal dominant Alzheimer's disease: a serial magnetic resonance imaging study. Alzheimers Dement 14, 43–53 (2018). [PubMed: 28738187]
34. Shahim P et al. Serum neurofilament light protein predicts clinical outcome in traumatic brain injury. Sci. Rep 6, 36791 (2016). [PubMed: 27819296]
35. Jucker M & Walker LC Propagation and spread of pathogenic protein assemblies in neurodegenerative diseases. Nat. Neurosci 21, 1341–1349 (2018). [PubMed: 30258241]
36. Bateman RJ et al. Autosomal-dominant Alzheimera's disease: a review and proposal for the prevention of Alzheimera's disease. Alzheimers Res. Ther 3, 1 (2011). [PubMed: 21211070]
37. Cairns NJ et al. Neuropathologic assessment of participants in two multi-center longitudinal observational studies: the Alzheimer Disease Neuroimaging Initiative (ADNI) and the Dominantly Inherited Alzheimer Network (DIAN). Neuropathology 35, 390–400 (2015). [PubMed: 25964057]
38. Tang M et al. Neurological manifestations of autosomal dominant familial Alzheimer's disease: a comparison of the published literature with the Dominantly Inherited Alzheimer Network observational study (DIAN-OBS). Lancet Neurol 15, 1317–1325 (2016). [PubMed: 27777020]
39. Thomas JB et al. Functional connectivity in autosomal dominant and late-onset Alzheimer disease. JAMA Neurol 71, 1111–1122 (2014). [PubMed: 25069482]
40. Folstein MF, Folstein SE & McHugh PR "Mini-mental state". A practical method for grading the cognitive state of patients for the clinician. J. Psychiatr. Res 12, 189–198 (1975). [PubMed: 1202204]
41. Morris JC The Clinical Dementia Rating (CDR): current version and scoring rules. Neurology 43, 2412–2414 (1993).
42. Wechsler D Wechsler Memory Scale-Revised: Manual (The Psychological Corporation, San Antonio, 1987).
43. Kuhle J et al. A comparative study of CSF neurofilament light and heavy chain protein in MS. Mult. Scler 19, 1597–1603 (2013). [PubMed: 23529999]
44. Disanto G et al. Serum neurofilament light: a biomarker of neuronal damage in multiple sclerosis. Ann. Neurol 81, 857–870 (2017). [PubMed: 28512753]
45. Carpenter B et al. Stan: a probabilistic programming language. J. Stat. Softw https://www.jstatsoft.org/article/view/v076i01 (2017).
46. Gelman A, Lee D & Guo J Stan: a probabilistic programming language for Bayesian inference and optimization. J. Educ. Behav. Stat 40, 530–543 (2015).

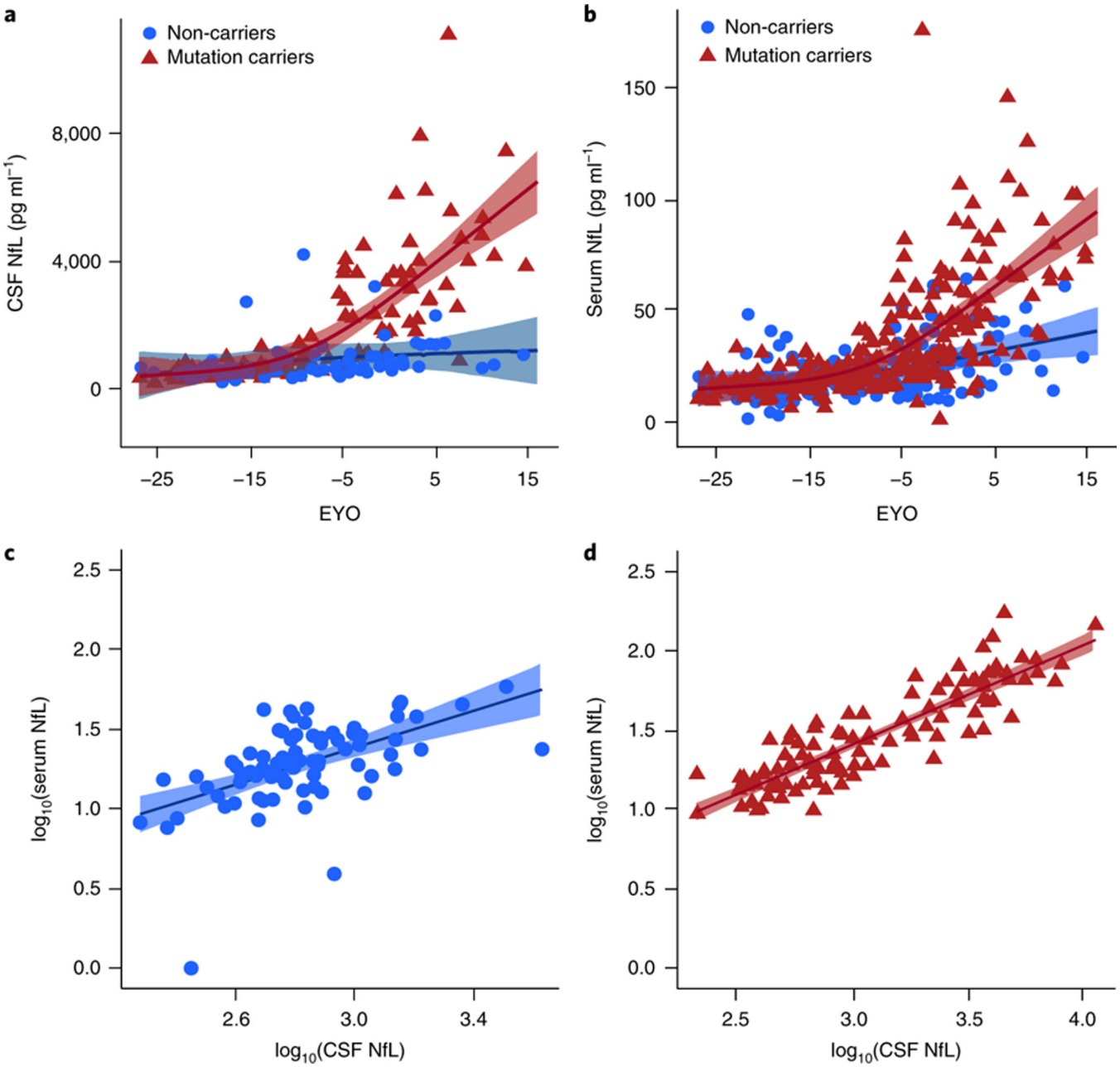

Fig. 1 |. CSF and serum NfL levels are highly correlated and divert between mutation carriers and non-carriers already in the presymptomatic phase.

a, CSF NfL values of non-carriers (blue, $n = 80$) and mutation carriers (red, $n = 107$) as a function of EYO. Shown is −27.5 until +15 years before or after EYO, respectively. **b**, Serum NfL for non-carriers ($n = 162$) and mutation carriers ($n = 243$) as a function of EYO. For **a** and **b**, the shaded areas represent the 99% credible intervals around the model estimates. The curves and credible intervals are drawn from the actual distributions of model fits derived by the Hamiltonian Markov chain Monte Carlo analyses (see Methods). The first EYO where non-carriers and mutation carriers differed was determined to be the first point where the 99% credible intervals around the difference distribution between non-carriers and

mutation carriers did not overlap 0 (−6.8 years before EYO for both CSF and serum, see Extended Data Fig. 1). Our analysis is influenced by the available number of participants. Thus, results do not represent absolute measures, but rather relative EYO points where we could detect effects given the limitations of sample size. **c**,**d**, Significant associations from LMEMs between CSF NfL and serum NfL in non-carriers ($n = 80$; B(s.e.m.) = 0.350(0.14), $P = 0.014$) and mutation carriers ($n = 107$; B(s.e.m.) = 0.612(0.05), $P < 2.0 \times 10-16$) were found.

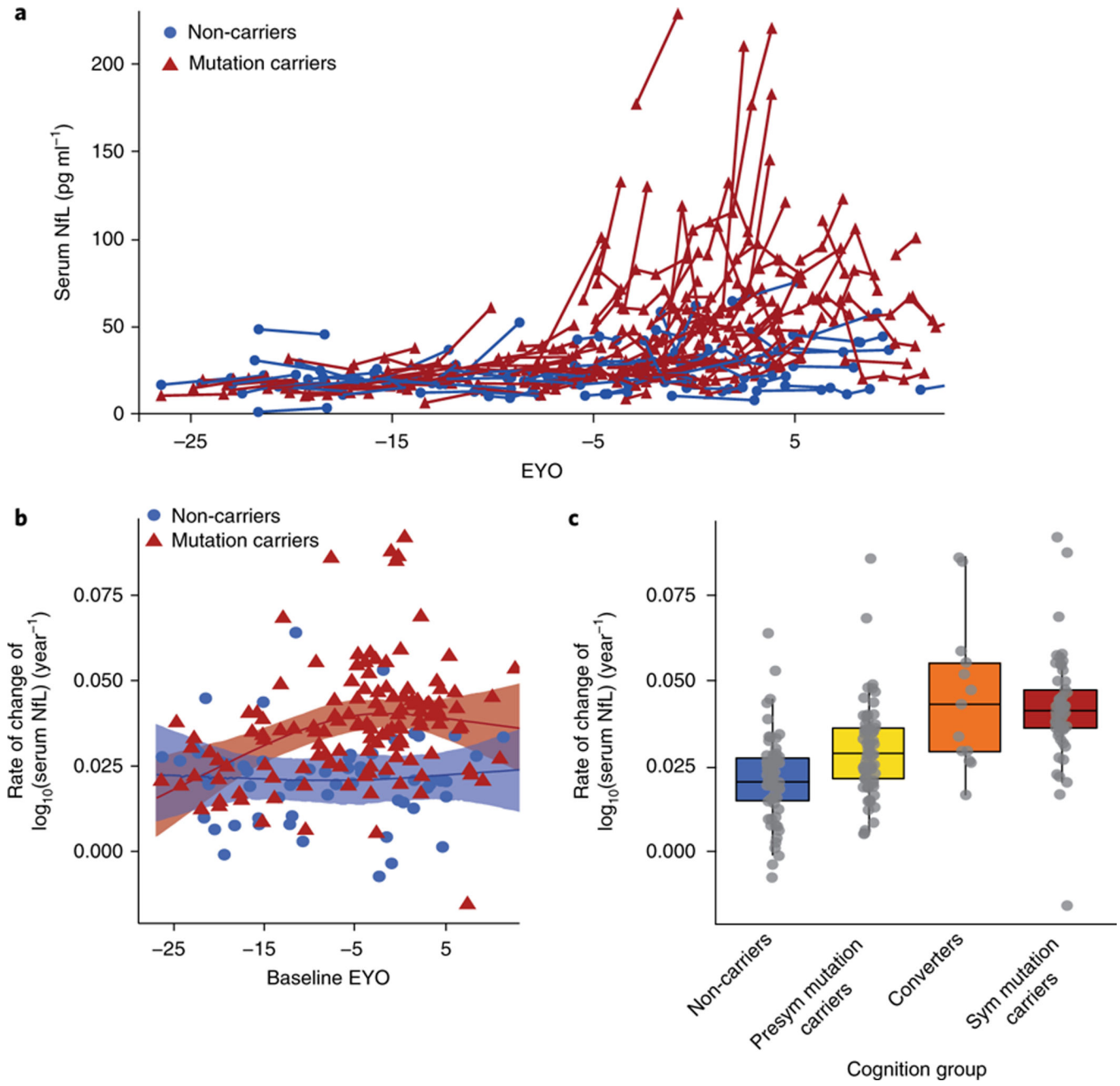

Fig. 2 |. Longitudinal serum NfL distinguishes mutation carriers from non-carriers very early in the presymptomatic disease process, with the NfL rate of change peaking in individuals converting from the presymptomatic to the symptomatic phase.

a, Spaghetti plot showing longitudinal serum NfL for non-carriers (blue, $n = 63$) and mutation carriers (red, $n = 133$) as a function of EYO. The displayed x axis range is limited to −27.5 until +12.5 years before or after EYO, respectively, to maintain blinding of some individuals contributing to this dataset. In addition, again to maintain blinding, the EYO of two participants (one mutation carrier and one non-carrier) was set to the mean of both EYO values. A logarithmic version of the spaghetti plot is shown in Extended Data Fig. 3a to better appreciate that changes between mutation carriers and non-carriers already occur at

presymptomatic levels. **b**, Estimated rate of change per year in serum NfL (see Methods for calculation) plotted against baseline EYO for mutation carriers and non-carriers (shown is −27.5 until +12.5 years). Individual random effect slope estimates are plotted as colored symbols. The shaded areas represent the 99% credible intervals around the model estimates. The curves and credible intervals are drawn from the actual distributions of model fits derived with the Hamiltonian Markov chain Monte Carlo analyses. The first EYO where groups (non-carriers and mutation carriers) differed was determined to be the first point where the 99% credible intervals around the difference distribution between non-carriers and mutation carriers did not overlap 0 (−16.2 years before EYO; see Extended Data Fig. 3b). An even earlier deviation of the two curves was calculated when linear regression analyses were performed (Extended Data Fig. 3c). **c**, Rate of change per year in serum NfL across four groups differing by mutation and cognitive status: non-carriers (blue, $n = 63$); presymptomatic (Presym) mutation carriers (yellow, $n = 65$) are individuals who scored as CDR= 0 across all visits; converters (orange, $n = 13$) are mutation carriers who scored as CDR= 0 at baseline and CDR> 0 at subsequent visits; symptomatic (Sym) mutation carriers (red, $n = 55$) are individuals who scored as CDR> 0 across all visits. The boxes map to the median, 25th and 75th quintiles, and the whiskers extend to 1.5 × interquartile range (IQR). Comparisons were done with LMEMs. Presymptomatic mutation carriers had a significantly higher annual rate of change compared to non-carriers (B(s.e.m.) = 0.009(0.003), $P = 6.71 \times 10^{-4}$). Converters had significantly higher rate of change compared to both non-carriers (B(s.e.m.) = 0.024(0.004), $P = 3.05 \times 10^{-7}$) and presymptomatic mutation carriers (B(s.e.m.) = 0.015(0.005), $P = 1.19 \times 10^{-3}$). Symptomatic mutation carriers had significantly higher rates of change compared to both non-carriers (B(s.e.m.) = 0.020(0.003), $P = 8.78 \times 10^{-12}$) and presymptomatic mutation carriers (B(s.e.m.) = 0.011(0.003), $P = 1.51 \times 10^{-4}$). There was no difference between converters and symptomatic mutation carriers (B(s.e.m.) = −0.004(0.005), $P = 0.445$).

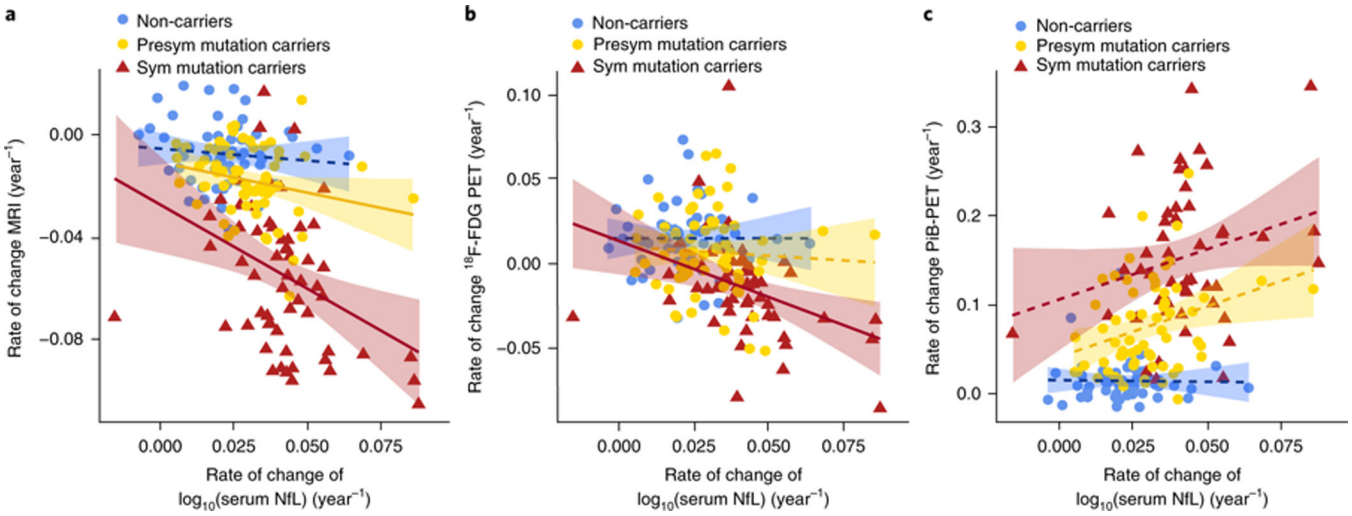

Fig. 3 |. Rate of change per year in serum NfL in mutation carriers mirrors rate of change in cortical thinning.

a, Relationship between estimated annual rate of change in serum NfL and estimated annual rate of change in precuneus cortical thickness for non-carriers, presymptomatic (Presym) mutation carriers, and symptomatic (Sym) mutation carriers (including converters to the symptomatic phase, see Fig. 2c). Results from LMEMs revealed a significant association in symptomatic mutation carriers ($n = 60$; B(s.e.m.) = −0.914(0.367), $P = 0.018$) and a close to significant association in presymptomatic mutation carriers ($n = 65$; B(s.e.m.) = −0.325(0.166), $P = 0.054$) but not in non-carriers ($n = 59$; B(s.e.m.) = −0.210(0.149), $P = 0.886$). Between-group comparison indicated that the rate of change in serum NfL was slightly more associated in symptomatic than in asymptomatic mutation carriers (B(s.e.m.) = −0.573(0.305), $P = 0.063$). **b**, Relationship between rate of change in serum NfL and rate of change in precuneus 18F-FDG PET. Using LMEMs, a positive association was only found in symptomatic mutation carriers ($n = 55$; B(s.e.m.) = −1.149(0.501), $P = 0.031$) but not in presymptomatic mutation carriers ($n = 64$; B(s.e.m.) = −0.227(0.456), $P = 0.620$) or non-carriers ($n = 55$; B(s.e.m.) = 0.161(0.347), $P = 0.465$). **c**, Relationship between rate of change in serum NfL and rate of change in precuneus amyloid-β-PET. Using LMEMs, no significant association in any of the three groups was found (non-carriers: $n = 57$; B(s.e.m.) = −0.468(0.547), $P = 0.403$; presymptomatic mutation carriers: $n = 64$; B(s.e.m.) = 1.248(1.000), $P = 0.216$; symptomatic mutation carriers: $n = 51$; B(s.e.m.) = 1.805(1.556), $P = 0.266$). The shaded area around each linear fit line represents one s.e.m. Note that not all participants with longitudinal NfL measurements had imaging parameters available, thus sample sizes (n) are slightly lower compared to those in Fig. 2c.

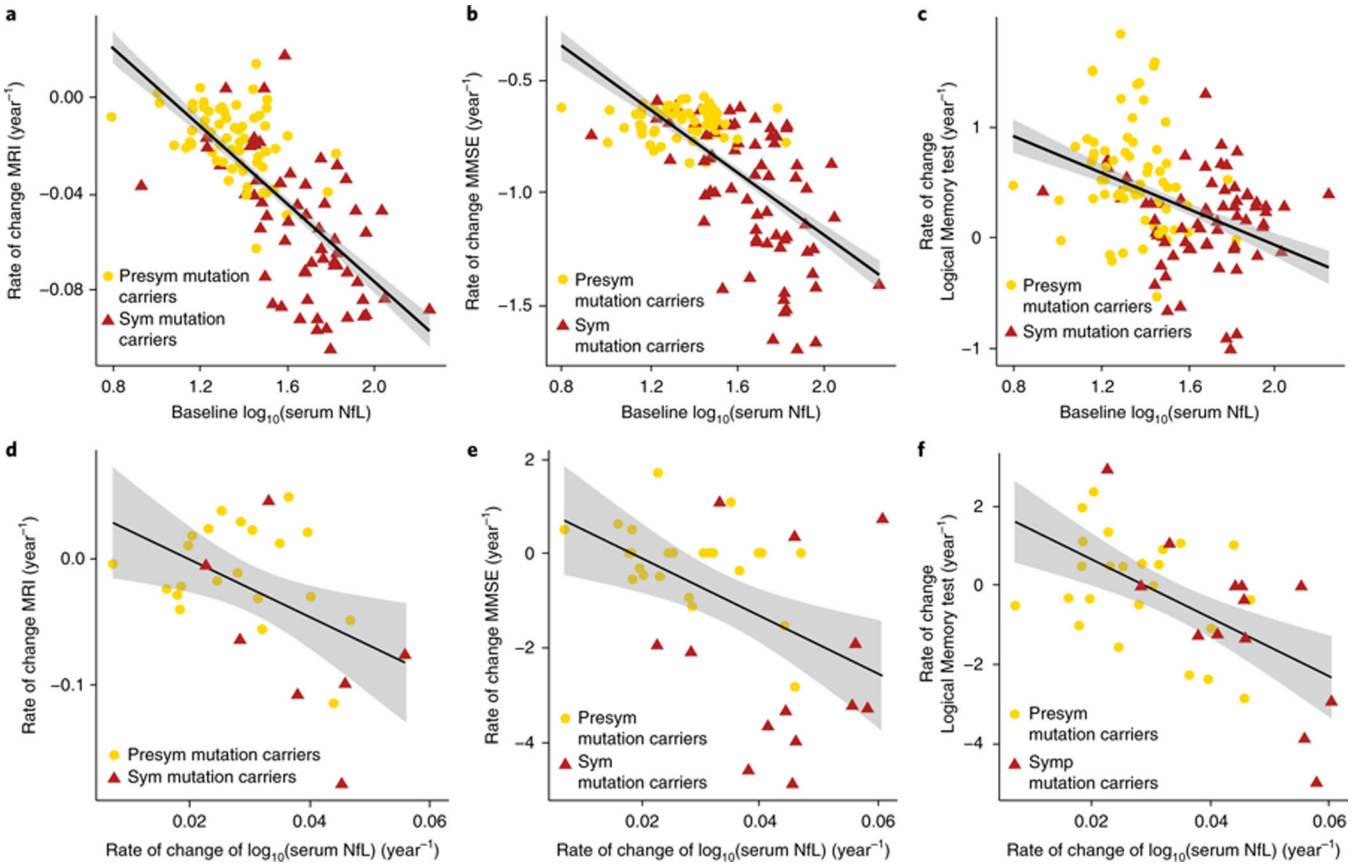

Fig. 4 |. Prediction of changes in cortical thinning and cognition by baseline serum NfL (retrospective prediction) and serum NfL rate of change (prospective prediction).

a–c, Higher baseline serum NfL levels were significantly associated with an increased rate of change in cortical thickness ($n = 125$; B(s.e.m.) = −0.105(0.013), $P = 4.47 \times 10^{-13}$) (**a**), MMSE ($n = 132$; B(s.e.m.) = −3.980(0.537), $P = 2.38 \times 10^{-11}$) (**b**), and Logical Memory test (immediate recall, $n = 133$; B(s.e.m.) = −1.478(0.502), $P = 0.004$) (**c**). A similar significance ($P = 0.015$) was obtained for the Logical Memory test delayed recall. LMEMs (see Methods) were run with all mutation carriers together ($n = 125$) because of the high degree of overlap in cognitive and biomarker levels between presymptomatic (Presym) and symptomatic (Sym) mutation carriers. However, at least for cortical thickness, separate analyses for presymptomatic and symptomatic mutation carriers were also significant ($n =$ 65, presymptomatic mutation carriers (yellow): B(s.e.m.) = −0.03(0.01), $P = 0.047$; $n = 60$, symptomatic mutation carriers (red): B(s.e.m.) = −0.10(0.03), $P = 0.002$). **d–f**, In a true prospective design, mutation carriers returning for follow-up visits after the last serum collection were included in the analysis. Individuals' rates of change in serum NfL levels predicted subsequent cortical thinning (**d**; $n = 30$; B(s.e.m.) = −1.867(0.769), $P = 0.024$). The same predictive associations were also significant for the MMSE (**e**; $n = 37$; B(s.e.m.) = −52.23(20.19), $P = 0.015$) and Logical Memory test scores (**f**; immediate recall, $n = 37$; B(s.e.m.) = −75.91(18.07), $P = 0.0002$). For descriptive purposes, presymptomatic and symptomatic mutation carriers are plotted in yellow and red, respectively. Note that not all participants with baseline NfL measurements had longitudinal MRI imaging and

longitudinal cognitive parameters available; thus, sample sizes (*n*) in **a**–**c** are slightly lower than those in Supplementary Table 2. This was also true for the mutation carriers returning for follow-up visits after the last serum collection (**d**–**f**). The shaded area around each linear fit line represents one s.e.m. from the LMEMs.